2024 IEEE/RSJ International Conference on Intelligent Robots and Systems (IROS)
October 14-18, 2024. Abu Dhabi, UAE

Strong Compliant Grasps Using a Cable-Driven Soft Gripper

Gregory Xie, Lillian Chin, Byungchul Kim, Rachel Holladay, and Daniela Rus

2024 IEEE/RSJ International Conference on Intelligent Robots and Systems (IROS) | 979-8-3503-7770-5/24/$31.00 ©2024 IEEE | DOI: 10.1109/IROS58592.2024.10801693

***Abstract*— The natural flexibility of soft robotic grippers allows for versatile and compliant grasping. However, this same flexibility can restrict the gripper's strength. Striking a balance between compliance and strength is essential for effective soft grippers. In this work, we present Flexible Robust Observant Gripper (FROG), a soft gripper that is both compliant and strong. We describe the mechanical design of the gripper, characterize the soft flexures used in the design, and analyze the grasp forces generated by the gripper. Utilizing the structure of the gripper, we develop feedforward grasp controllers and a classifier to distinguish between grasp types. Grasping experiments show that FROG can effectively grasp a variety of objects, including very soft or delicate items. Holding force tests show that our gripper can conform to the grasped object and exert large grasp forces.**

I. INTRODUCTION

Soft grippers allow robots to passively accommodate for uncertainty in the shape and pose of the objects they are manipulating by introducing compliance at the point of interaction between the robot and its environment. However, this same compliance limits the grasp forces that these grippers can exert [1]. This is unacceptable in many real-world manipulation tasks, where the robot must operate in unstructured environments while still exerting significant forces through the grasped object [2, 3]. An ideal gripper would remain compliant before and during the formation of a grasp, and then stiffen during the grasp to apply significant forces.

This desired stiffness modulation can be achieved either through active or passive methods [4]. Active methods use actuators to change the mechanical properties of the soft gripper, such as layer/particle jamming [5, 6, 7] or antagonistic actuation [8, 9]. These methods often suffer from the inability to significantly vary the stiffness and slow response times [10]. Passive methods rely on contact constraints to control stiffness, as seen in rigid underactuated hands [11]. However, applying this method to soft hands is challenging due to their inherent lack of structure, further complicating control and proprioception.

To address these challenges, we introduce Flexible Robust Observant Gripper (FROG), a soft gripper that passively stiffens through contact (Fig.1). By selectively replacing soft elements with comparatively rigid ones, the number of effective degrees-of-freedom in the structure is reduced [12, 13]. This way, each object contact constrains more of the system, increasing the change in stiffness and allowing for stronger grasps.

Fig. 1: Flexible Robust Observant Gripper (FROG) mounted on a Universal Robots UR5, with the cable path highlighted in green (left). FROG is simultaneously strong and compliant, shown lifting a 10 lb (4.5 kg) dumbbell (middle) and being deformed by a plastic bat (right).

Replacing soft elements with stiffer ones streamlines the relationship between the actuator and the grasp, facilitating actuator-based proprioception. While soft grippers are adept at blindly grasping objects, they cannot provide information about how the object was grasped without complicated sensing structures [14, 15, 16, 17]. Actuator proprioception for these grippers is impractical due to difficulties in measuring actuator effort and/or displacement and soft material drift over time.

To further simplify the relationship between actuator and grasp quantities, FROG is actuated by cables [18, 19, 20]. Common bio-inspired cable routing paths often require the use of large cable tensions as the cables run close to the (finger) joints and provide low mechanical advantage. FROG uses an alternative cable routing [21] to increase mechanical advantage, enabling the use of a direct drive motor [22] to estimate cable tension and allow for control of actuator displacement and effort.

FROG achieves hardware complexity on par with other soft grippers while providing additional control over the grasp force and proprioception of the grasp type through

This work was supported by NSF EFRI under Grant 1830901 and the Gwangju Institute of Science and Technology.

Gregory Xie, Byungchul Kim, Rachel Holladay, and Daniela Rus are with the MIT Computer Science and Artificial Intelligence Laboratory (CSAIL), Massachusetts Institute of Technology, Cambridge, MA 02139 USA. (email: {gregoryx, bckim, rholladay, rus}@csail.mit.edu)

Lillian Chin was the MIT Computer Science and Artificial Intelligence Laboratory (CSAIL), Massachusetts Institute of Technology, Cambridge, MA 02139 USA at the time of this work. Her current address is the Department of Electrical and Computer Engineering, The University of Texas at Austin, Austin, TX 78712 USA. (email: ltchin@utexas.edu)

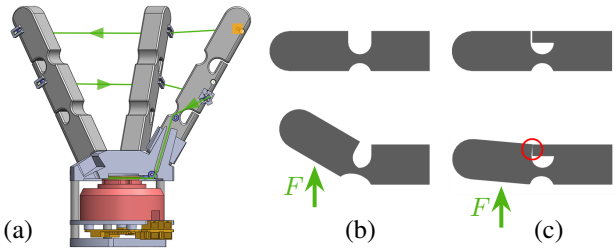

Fig. 2: (a) Section view of FROG showing three of the five fingers. The motor is shown in red, motor driver in yellow, spool in orange, and a section of cable in green. Arrows on the cable path show the direction of travel when closing the gripper. An orange square marks the location at which the cable is terminated at the finger. (b) Without a backstop, large deformations of the flexure joints limit the fingertip force. (c) Contact with a backstop greatly increases the stiffness of the joint, allowing for more forceful fingertip grasps.

the integration of simple control and sensing algorithms. We develop a feedforward grasp force controller and a stiffness-based classifier to distinguish between grasp types, where grasp types are defined by the finger segments in contact with the object. We characterize the dynamic properties of the joints used in each finger and the holding force that the gripper can exert. Finally, we demonstrate our gripper by manipulating a wide variety of items, including fragile and soft objects.

This paper contributes the following:

1) Design and fabrication of Flexible Robust Observant Gripper (FROG), a cable-actuated soft gripper that can robustly conform to grasped objects and improves proprioception and control.
2) Development of two simple feedforward grasping modes to allow FROG to grasp delicately or forcefully and characterization of the strength of FROG's grasps.
3) Development and evaluation of a stiffness-based proprioception algorithm that can estimate the grasp type.
4) Demonstration of FROG's grasping performance on everyday objects and the effectiveness of FROG's soft grasp mode on fragile objects.

II. SYSTEM DESIGN

In this section we describe FROG. We first introduce the hardware design that incorporates stiffer elements into the gripper, allows for deformation through the addition of flexural joints, and enables actuator proprioception through a direct-drive cable mechanism. Next, we characterize the flexural joints to inform the design of the feedforward grasp controllers and a grasp type proprioception algorithm. We then present the grasp controllers and the proprioception algorithm. Finally, we analyze the grasp forces generated by the gripper.

A. Hardware Design

Our gripper design has 5 fingers, driven by a single tension-controlled cable (Fig.1-a). Each finger is soft, with a Shore hardness of 72A, and is 3D printed in one piece (using Carbon EPU 40). Instead of making the entire finger thin, which would allow for continuous bending, we add structure by thickening the finger and adding two flexure joints (Fig.2-b). This splits the finger into three links. Because the stiffness of the flexure joint is low compared to the link stiffness, deformations are mostly localized at the joints. The increased structure allows contacts to effectively constrain and stiffen the finger and allows for actuator proprioception. The flexures are 4.3 mm thick and 15 mm wide, with a notch radius of 6 mm.

The flexures also support two secondary motions, side-to-side and twisting, enabling the fingers to conform to surfaces that are not normal to the nominal link surface. By incorporating backstops in the flexures, the finger's stiffness is enhanced, enabling significant force application in grasps where contact is made on the distal links (Fig.2-c). The fingers are glued into a 3D printed base (Markforged Onyx) with two-part epoxy.

As shown in Fig.2-a, the closure of the fingers is actuated by a single UHMWPE (Ultra-high-molecular-weight polyethylene) cable routed around the fingers. This cable routing is inspired by Kim et al. [21] and allows the gripper to be actuated with a lower cable tension than typical cable-actuated grippers. This is due to the longer joint-cable distance and the cable applying two tension forces each time it traverses a finger.

From the spool, the cable is routed through the proximal flexure's center of rotation to minimize additional torque on the joint and then goes through the cable guides on the proximal links of the fingers. The cable is then routed through a PTFE (polytetrafluoroethylene) Bowden tube and the cable guides of the distal links before it is terminated at one of the distal links. From the actuator's perspective, the stiffness of the proximal joint is less than that of the distal joint. This leads to significant movement in the distal joint only after the proximal link has established contact.

The cable guides were designed for a cable tension of 10 N; each one consists of two bearings (682ZZ) on dowel pins and a PTFE guide tube that are glued into a 3D printed housing (Carbon UMA 90) using cyanoacrylate (CA) glue. CA glue is also used to glue the cable guide assembly into the fingers. Features on the housing prevent the cable from falling off the roller if it becomes slack.

Off-the-shelf polyester bellows between the fingers prevent grasped objects from directly contacting the cables. The bellows are attached to the fingers with double sided tape.

The cable is pulled by a direct drive brushless DC gimbal motor (T-motor GB54-1, mjbots moteus r4.11). The spool has a radius of 11.5 mm, and is sized so that the motor can continuously pull the cable to the design tension of 10 N. The spool is designed to ensure subsequent wraps of the tendon completely overlap with previous ones, allowing FROG to compensate for changes in spool diameter as the cable is wrapped. As the typical current through the motor is less than 2 A, the motor driver's stock current sense resistors (0.5 mΩ) are replaced with larger ones (5 mΩ). The direct drive

actuator allows for control over cable tension and position, increasing the capability of FROG when grasping objects.

Overall, the gripper is 180 x 170 mm, with a ideal maximum grasp diameter of 130 mm. Because of friction, typically a maximum grasp diameter of only 110 mm is achievable. The bellows and finger thickness limit the minimum grasp diameter to 38 mm.

B. Dynamic Flexure Characterization

Understanding how the flexure joint torques evolve over time informs how time-varying effects should be compensated for in the design of the controllers and proprioception algorithm. We characterize the joint torque in response to the displacement of the flexure. As seen in Fig.3-a, we mount test flexures to a custom torsion testing system, consisting of a servo (Dynamixel MX-28) and a force/torque sensor (ATI gamma SI-32-2.5). The force/torque sensor measures the reaction torque generated when the servo arm displaces the flexure.

Measuring the steady-state torque needed to displace a flexure, we see that it is relatively linear with displacement until approximately 1.25 radians (Fig.3-b). This suggests that a linear dynamical model will model the flexure's dynamic response well. Nonlinear behavior at large displacements is expected because of the elastomeric material used.

We choose a Generalized Maxwell model [23] with five time constants, which we fit using MATLAB's System Identification Toolbox using data from exponential chirps (0.25 - 0.0005 Hz, 0.35 radian amplitude, $\pi/4$ radian offset) on five flexures. We verify our model by comparing the real and predicted responses to a step displacement of $\frac{\pi}{4}$ radians (Fig.3-c). We find good agreement, with a MSE of $1.2 \cdot 10^{-5}$ N^2-m^2 over 500 seconds, roughly 5x the longest time constant in the model.

Overall, we observe a relatively linear response and significant amounts of stress relaxation. The linearity of the response suggests that we will be able to use a stiffness-based proprioception algorithm (Sec. II-D). To avoid having to account for viscoelastic effects in our proprioception algorithm, we choose a closing period which makes the system quasi-static while still allowing for reasonably quick grasps. We choose a closing period of 5 seconds, corresponding to a motor velocity of 2π rad/s, as it is more than 3 times larger than all but the largest time constant in the model. The chosen closing period should greatly reduce the amount of stress relaxation after the flexures stop moving, which we validate in Sec. III-A by measuring how the holding force changes over time.

C. Grasp Mode Design

FROG's direct drive actuator allows for measurement and control over actuator displacement and effort. To show how these properties increase the types of objects that FROG can manipulate, we develop example controllers for two grasp modes: a soft grasp and a hard grasp. These grasps allow FROG to delicately grasp fragile objects using the soft grasp mode or to forcefully grasp rigid objects using the hard grasp

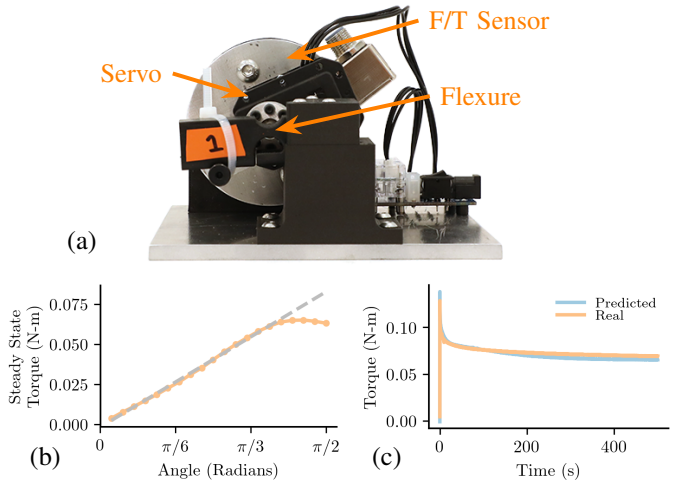

Fig. 3: (a) The torsion testing system used to test flexures. (b) Steady state torque of a flexure. The steady state torque is linear with displacement until 1.25 radians, shown by the dashed line. (c) Step responses predicted by the identified model and measured on the testing system.

mode. We assume the choice of grasp mode is determined by the user or a higher-level planner.

For these controllers, we spool the cable at a set velocity (2π rad/s). Every control cycle, we measure the current cable position p and the controller determines the maximum tension the motor is allowed to exert $f(p)$.

The controller for the hard grasp mode is simple: we command the motor to spool the cable with $f(p) = f_{max} = 10$ N. This exerts the largest grasp forces, resulting in the strongest grasp possible.

For the soft grasp mode, we leverage the physical consistency of our finger design and fine control over gripper actuation effort to do approximate feedforward force control. We assume that all movement stops after contact. We define $f_{nc}(p)$ to be the tension force needed to close the gripper without contact at a cable position p. We measure $f_{nc}(p)$ by closing the gripper with no object contact (Fig.4-b). During a soft grasp, we command the motor to spool the cable with $f(p) = f_{nc}(p) + c + \epsilon$, where c is a experimentally determined offset to ensure the gripper consistently closes in all orientations and ϵ is a small user-specified quantity corresponding to grasp force. Empirically, we observe that $c = 0.3$ N and $\epsilon = 0.1$ N generates grasps that can pick up a variety of delicate and lightweight objects.

Since the grasp force is a function of both the cable tension and contact locations, we cannot do true feedforward force control as we do not know where objects contact the fingers of FROG. Despite the range of possible contact forces, we demonstrate in Sec. III-C that FROG is still able to grasp a variety of fragile objects using the soft grasp mode. In Sec. II-D we describe why we cannot estimate contact locations in the soft grasp mode.

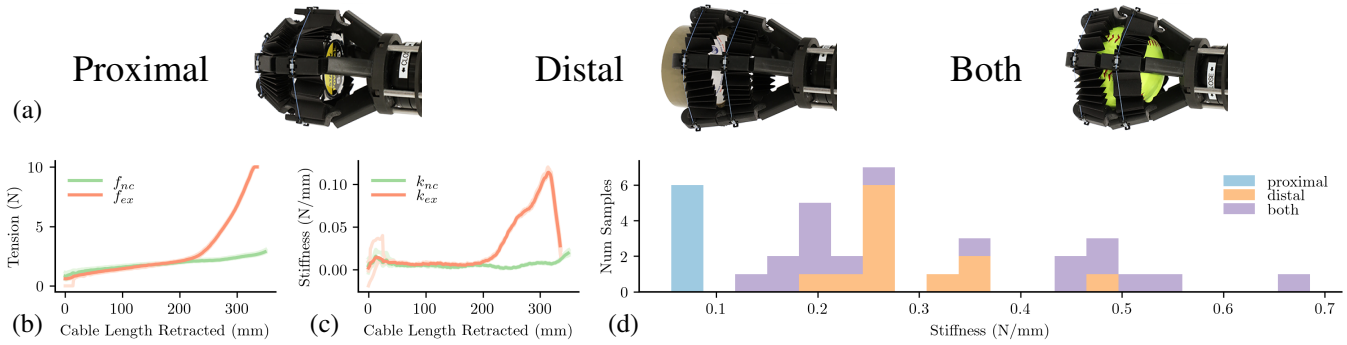

Fig. 4: (a) Examples of the three grasp types we attempt to differentiate between using our grasp classifier. Cable tension (b) and finger stiffness (c) over 10 trials in a grasp with no contact and in an example grasp with both proximal and distal contact, shown in green and orange respectively. Each trial is shown in a shaded line with the average shown in the darker line. Because the trials are very repeatable, the trajectories overlap. (d) Distribution of maximum finger stiffness for different grasp types.

D. Grasp Type Proprioception

To show how FROG's structure increases the information implied from its actuator, we demonstrate the effectiveness of a simple stiffness-based proprioception algorithm.

As the links of an underactuated finger come into contact with an object, the stiffness seen from its actuator changes [24]. An example is shown in Fig.4-c for a grasp with object contact on all links. The actuator stiffness (k_{ex}) closely follows the grasp with no contact (k_{nc}) until contact is made, after which the stiffness increases. Previous work has focused on fingers with rigid links and have used this effect to estimate the exact location of contact on the links of an underactuated finger [25, 26]. We observe that similar techniques can be used as long as the joints are significantly less stiff than the links.

Rather than analytically computing the exact location of contact, we take a more data-driven approach to estimate the grasp type due to the difficulty of modeling our flexible link fingers. We define three grasp types (Fig.4-a):

- **Proximal**: All fingers are contacting the object with the proximal link
- **Distal**: All fingers are contacting the object with the distal link
- **Both**: All fingers are contacting the object with both links

We limit ourselves to the case where all fingers contact the object with the same contact state (e.g. all fingers contact the object on their distal links, or a "distal" grasp). However in practice, it is possible for different fingers to contact the grasped object with different contact types. For example, 3 fingers could contact the object on their distal links while the other 2 fingers contact the object on both their proximal and distal links. In this example, we expect this to result in a grasp stiffness between the stiffness of a "distal" and "both" grasp. During both the training and test phases (Sec. III-B), if FROG grasps an object with mixed contact types, we do not include the trial. Additionally, we do not include trials with grasps that are not stable.

We only perform grasp classification in the hard grasp mode because the tension limit in the soft grasp mode prevents us from measuring the stiffness of the fingers after contact. While the gripper is closing in the hard grasp mode, we measure and low-pass filter the instantaneous finger stiffness $k(p) = \frac{\delta f(p)}{\delta p}$, recording the maximum instantaneous stiffness. We use the maximum stiffness rather than the final stiffness because at the end of the grasp, the fingers continue to move after the maximum tension has been reached due to viscoelastic effects. We use a moving average filter with a window size of 20 samples (0.1 seconds).

We collect the maximum stiffness from different grasps on 8 training objects for a total of 35 data points (Table I). Items are grasped more than once if FROG is able to grasp the item with multiple grasp types or if the orientation of the item significantly changed how the gripper contacts the object. The measured stiffnesses, classified by grasp type, are shown in Fig.4-d.

After a grasp, we use the maximum instantaneous stiffness to classify the grasp using a k-nearest neighbors classifier ($k = 5$). We evaluate the accuracy of our classifier in Sec. III-B. The results and test objects are shown in Table II.

E. Grasp Force Analysis

Because FROG's actuator is coupled to all of its fingers, the geometry of an object influences the forces that are exerted on it during a grasp. To show that FROG is able to consistently grasp a wide variety of objects, we analyze the extent to which the sum of contact forces changes in response to object geometry. We focus our analysis on "distal" grasps using the hard grasp mode as we observe that these grasps occur frequently in common manipulation

Training Items
Baseball, Plastic Peach, Plastic Pear, Can of Tuna, Plastic Bottle, Metal Tumbler, Spray Can, Aluminum Stand

TABLE I: The training objects used to fit the grasp classifier.

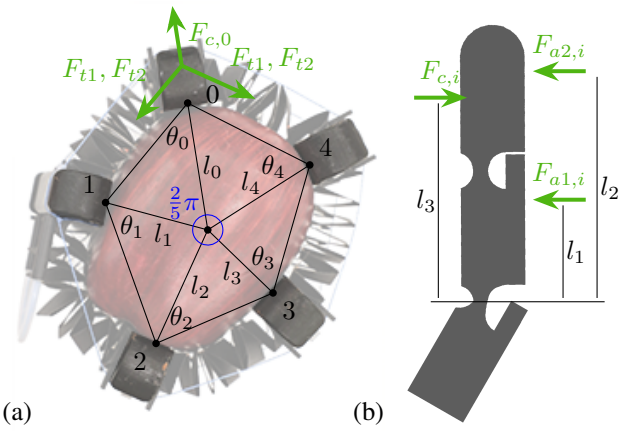

Fig. 5: (a) Top view of FROG grasping an apple and the planar approximation we use for grasp force analysis. (b) Free-body diagram of one finger during a grasp with contact on the distal link. We assume all fingers are approximately vertical in our grasp force analysis.

environments, especially table-top manipulation (Sec. III-B).

We assume that the fingers are approximately vertical (seen in Fig.5-b), the flexure has zero stiffness, each finger only moves radially, and that all objects contacts happen at the middle of each distal link. This idealized setting allows us to analyze the grasp in a plane, shown in Fig.5-a. We believe these assumptions are reasonable as the fingers can only deviate up to $\pi/6$ radians from vertical (when the gripper is completely open), deforming the flexures requires a maximum of 30% of the hard grasp tension (Fig.4-b), and the flexures are designed to primarily allow flexion of the fingers.

Using the free-body diagram shown in Fig.5-b, we balance moments to relate the contact force of finger i ($F_{c,i}$) to the forces from the cable tension:

$$F_{c,i} = \frac{F_{a1,i}\ l_1 + F_{a2,i}\ l_2}{l_3}. \tag{1}$$

For FROG, $l_1 = 31$ mm, $l_2 = 73$ mm, and $l_3 = 63$ mm.

Next, we look at the top view of the grasp (Fig.5-a) and balance the forces on each finger radially to find that:

$$F_{a1,i} = F_{t1}(\cos(\theta_i) + \cos(\frac{3\pi}{5} - \theta_{i-1})) \tag{2}$$

$$F_{a2,i} = F_{t2}(\cos(\theta_i) + \cos(\frac{3\pi}{5} - \theta_{i-1})) \tag{3}$$

where F_{t1} and F_{t2} are the tensions in the bottom and top section of the cable. Since the cable passes through a bowden tube between the bottom and top sections, $F_{t1} = e^{\mu\theta}F_{t2}$ [27], where $\theta = \pi$ radians due to the design of the gripper. We assume the coefficient of friction between the cable and the bowden sheath is $\mu = 0.075$ [27]. Because the bottom cable section is connected to the motor through pulleys and we are grasping using the hard grasp mode, the tension is the same as the tension at the motor ($F_{t1} = F_t = 10$ N).

Combining (1) with (2) and (3):

$$F_{c,i} = \alpha F_t(\cos(\theta_i) + \cos(\frac{3\pi}{5} - \theta_{i-1})) \tag{4}$$

where $\alpha = \frac{l_1 + l_2/e^{\mu\theta}}{l_3}$. Since each finger can only apply a positive (or zero) force on the object, $\cos(\theta_i) \geq 0$ and $cos(\frac{3\pi}{5} - \theta_i) \geq 0$. Combining and simplifying the two constraints, we find that: $\frac{\pi}{10} \leq \theta_i \leq \frac{\pi}{2}$. Because the cables trace a closed curve, we add a loop closure constraint. Using the sine rule, we find that the distance from the contact point i to the center (l_i) is:

$$l_{i-1}\sin(\theta_{i-1})/\sin(\frac{3\pi}{5} - \theta_{i-1}). \tag{5}$$

For loop closure, $l_5 = l_0 = C$.

We can now find the minimum grasp force by solving the optimization problem:

$$\begin{aligned} \min_{\theta} \quad & \alpha F_t \sum_{i=0}^{4} \cos(\theta_i) + \cos(\frac{3\pi}{5} - \theta_i) \\ \text{s.t.} \quad & \frac{\pi}{10} \leq \theta \leq \frac{\pi}{2} \\ & l_i = l_{i-1}\sin(\theta_{i-1})/\sin(\frac{3\pi}{5} - \theta_{i-1}) \\ & l_5 = l_0 = C \end{aligned} \tag{6}$$

To find the maximum grasp force, we maximize the cost function instead. We solve the optimization problem using Drake's MathematicalProgram [28]. Since the problem is nonlinear, we solve with $10,000$ random seeds sampled from $\pi/10 \leq \theta_{init} \leq \pi/2$ and take the best solution. We see that the grasp force during a hard grasp can vary between 70 N and 83 N depending on object geometry.

From this analysis, we expect around a 20% variance in the grasp force during a "distal" grasp due to object shape. This suggests that FROG will be able to generate consistent grasps on a variety of objects. In practice, we expect the range of grasp forces to both decrease and widen, mainly due to the stiffness of the flexures.

III. PERFORMANCE CHARACTERIZATION

We evaluate FROG's performance with three experiments. First, we test the strength and gentleness of FROG by measuring its holding force in the hard and soft grasp modes. Next, we evaluate the performance of our grasping proprioception algorithm on household objects. Finally, we demonstrate FROG's ability to grasp fragile objects. Through these experiments, we see that FROG is able to forcefully or softly grasp a variety of objects and estimate how the objects are being grasped.

A. Holding Force

We evaluate the strength of the grasps generated by FROG by measuring the force needed to pull out a grasped object using a tension testing machine (Instron 5944). We attach FROG to the stationary lower test fixture and the test object to the moving upper test fixture (Fig.6-a). The test object is lowered into the gripper until just before the object

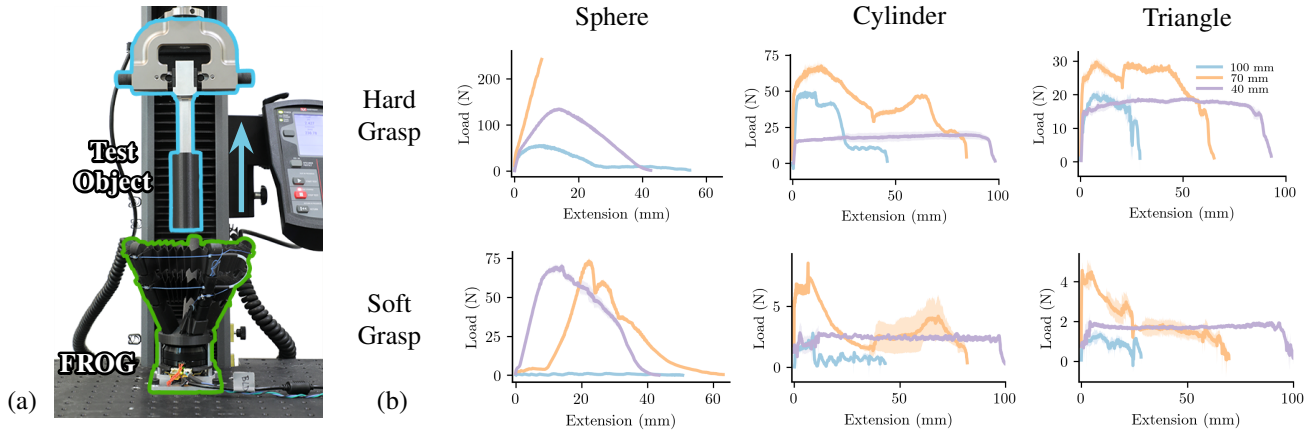

Fig. 6: Holding force characterization. (a) The test setup used to measure the holding force. FROG and a test object in the upper fixture are outlined in green and cyan, respectively. The arrow shows the direction of object travel during the test. (b) The average holding force for each test object over 5 trials with the standard deviation shown by the shaded area. Because the grasps are very repeatable, the standard deviations are small. The test is terminated early if a force limit (250 N) is reached. Note that the scales vary across objects and grasp mode.

contacts any part of the gripper and before any of the gripper fingers contact the mounting stem during a hard grasp. The same object location is used for the soft and hard grasp tests. The object is grasped using one of the two grasp modes and the object is pulled out of the gripper by moving the upper test fixture at 1 mm/s. The test is terminated after the object leaves the gripper or when a maximum load of 250 N is exceeded.

As explained in Sec. II-C, we must specify an ϵ that controls the grasp force during a soft grasp mode. Due to abnormal wear on the cable prior to this test, a soft grasp ϵ of 0.5 N was needed to close the gripper. We use $\epsilon = 0.6$ N in the test, which is equivalent to $\epsilon = 0.1$ N due to the additional friction.

We test three different object geometries in three different sizes - spheres, cylinders, and triangular prisms with a diameter or side length of 40 mm, 70 mm, and 100 mm. The cylinders and triangular prisms are 100 mm tall. We chose these objects as they test a variety of different grasps. The cylinders test force closure grasps where the fingers cannot wrap around the top of the object. The spheres additionally test form closure grasps where the fingers are able to wrap around the top of the object. The triangular prism serves as an adversarial object that contacts the bellows of FROG.

As shown in Fig.6-b, FROG is able to grasp the medium-sized objects the strongest, with the maximum holding force reaching $>$ 250 N, 65 N, and 30 N for the 70mm sphere, cylinder, and triangular prism, respectively. The sharp corners of the triangular prism interfere with the cable and reduce the cable tension, reducing the grasp force that FROG is able to exert. Form closure grasps greatly increase the holding force, as friction is no longer needed to resist external forces. FROG performs worse at holding objects close to its minimum or maximum diameters.

The holding force for the form closure grasps on the various spheres show a distinct peak as the test object is pulled past the fingers. The 70 mm and 100 mm cylinders show distinct regions before and after the proximal links lose contact at around 40 mm and 24 mm of extension, respectively. Overall, these results support that FROG is capable of generating strong grasps with high holding forces.

Next, we compare how the holding force in a force closure grasp compares to the predicted grasp forces in Sec. II-E. In a force closure grasp the holding force is related to the grasp force through a friction coefficient, we assume $\mu_{grasp} = 0.3$ (Carbon EPU 40 on Markforged Onyx). For the 40 mm cylinder and triangle, we predict a holding force between 21 and 25 N. We observe an average grasp force of 18 and 17 N for the cylinder and triangle, respectively, showing good agreement.

We then use the holding forces for force closure grasps in the soft grasp mode to confirm that the soft grasp mode greatly decreases the grasp force. Assuming the same friction coefficient, this results in an maximum contact force of 6 N per finger in the soft grasp mode. For grasps where only the distal links contact the test object, the average contact force is 1.3 N per finger. This suggests that the soft grasp mode would be well suited to gentle grasping of fragile objects, which we demonstrate in Sec. III-C.

We note that the holding forces for the 40 mm and 70 mm sphere in the soft grasp mode remain relatively large since these are form closure grasps. In addition, the friction in the system may have prevented the motor from correctly regulating the cable tension as the objects push past the fingers, resulting in abnormally high holding forces for these grasps.

To validate that the closing period chosen in Sec. II-B allows for quasi-static operation of the gripper, we test if the holding force in the soft grasp increases over time. If the holding force increases over time, fragile items could be damaged in the grasp. We test using the soft grasp mode because we expect the percent increase in grasp force to be

bigger than in the hard grasp mode.

We measure the holding force on the 40 mm cylinder 4 times, each measurement taking 120 seconds. Immediately after each measurement, we regrasp the cylinder and maintain the grasp for 300 seconds until the next measurement. For each measurement, we calculate the average holding force. The test lasts for 23 minutes in total and shows no discernible relationship between time and holding force, showing that FROG behaves quasi-statically.

B. Grasp Type Proprioception

We evaluate the accuracy of FROG's grasp classifier on 21 unique test objects, listed in Table II. Objects in random orientations were grasped off a table to test the classification of "distal" and "both" grasps. In this specific setting (table-top manipulation), we observe that "proximal" grasps are hard to obtain so we test the classifier by handing the gripper objects to grasp. We believe "proximal" grasps would be more common in human-robot handoffs or catching. We do not count trials where the grasp is not stable or where the grasp has a mixed grasp type. For a given object, each possible grasp type is tested 5 times.

We observe that the classifier is able to identify the type of grasp 67% of the time. Most errors are from misclassifying "distal" grasps as "both" grasps and vice versa. We expect these grasp types to be the most likely to be misclassified as the stiffness distributions for these two grasp types are close and overlap (Fig.4-d).

The classifier performs poorly with compliant and objects that are not radially symmetric. Compliant objects like the foam block reduce the grasp stiffness because the object stiffness appears to be in series with the actuator. Objects like the multimeter, computer mouse, stacked construction blocks, and toy pig are not radially symmetric and cause the fingers to twist as they make contact with the object, which may change the grasp stiffness. Despite being rigid and radially symmetric, we believe the can of WD40 is misclassified because it is near the grippers minimum grasp diameter.

Compared to the original approach taken by Belzile and Birglen [24], we see similar limitations in regard to object and grasp symmetry. In later work [26, 25], the authors are able to detect the exact contact location along a finger, but require one actuator per finger. In all implementations, the authors do not evaluate their approach with respect to compliant objects.

Overall, the experiment shows that the classifier works well on rigid objects that have an approximate radial symmetry.

C. Fragile Object Grasping

Finally, we demonstrate the FROG's ability to grasp fragile objects, shown in Fig.7. We grasp objects that are fragile due to their geometry, brittleness, or low stiffness using FROG's feedforward soft grasp mode. We set $\epsilon = 0.1$ N for all of these tests. All objects were grasped off a table.

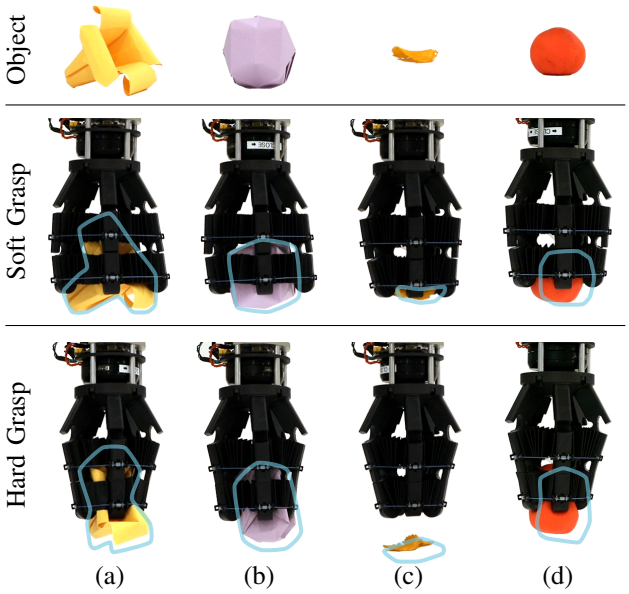

Fig. 7: FROG's structure and actuator allow it to easily grasp fragile objects. Rows show, from top to bottom, the object, the result after a soft grasp, and the result after a hard grasp. Columns show (a) grasping a paper flower, (b) paper ball, (c) potato chip, and (d) ball of Play-Doh. Objects are highlighted in the gripper for clarity.

We first grasp two origami objects, a paper flower and a paper ball, shown in Fig.7-a and Fig.7-b, respectively. Both objects are crushed when grasped with the hard grasp mode and are undamaged when grasped with the soft grasp mode. Based off of tests done in Hughes et al. [29] and Maruyama et al. [30], we demonstrate FROG on potato chips (Fig.7-c). The hard grasp mode causes the potato chip to fracture and the grasp to fail while the soft grasp mode is able to lift the chip without damage. Finally, we show FROG grasping a ball of Play-Doh without significant deformation using the soft grasp mode (Fig.7-d). Once we switch to the hard grasp mode, the ball is squished. This demonstrates the effectiveness of our soft grasp mode in grasping fragile and soft objects.

IV. DISCUSSION

In this work we present FROG, a soft gripper capable of generating robust grasps that can be strong or gentle using its direct drive actuator. FROG is able to leverage the structure of its fingers to enable the use of a stiffness-based proprioception algorithm, allowing it to classify the type of grasp it has on an object. These additional capabilities come without large increases in hardware complexity and with only the addition of simple control and sensing algorithms.

In the future, we are interested in further exploring the use of the time series stiffness information from a grasp to estimate flexure angles and optimizing the flexure design for stiffness-based proprioception.

Test Object	Proximal	Distal	Both	Overall
Bottle of Bleach	-	-	5/5	5/5
Computer Mouse	-	0/5	-	0/5
Container of Play Doh	-	4/5	3/5	7/10
Container of Wet Wipes	-	4/5	5/5	9/10
Foam Block	-	0/5	-	0/5
Large Roll of Tape	-	4/5	-	4/5
Milk Frothing Pitcher	-	4/5	-	4/5
Mug	-	3/5	-	3/5
Multimeter	-	0/5	-	0/5
Plastic Apple	5/5	5/5	-	10/10
Plastic Orange	5/5	5/5	-	10/10
Plastic Toy Pig	-	2/5	0/5	2/10
Plastic Wine Glass	-	4/5	4/5	8/10
Small Can of WD40	-	0/5	-	0/5
Small Hand Clamp	-	2/5	-	2/5
Small Roll of Tape	-	5/5	-	5/5
Softball	-	5/5	4/5	9/10
Spam Can	-	5/5	-	5/5
Stacked Large Construction Blocks (3)	5/5	0/5	-	5/10
Tape Measure	5/5	4/5	-	9/10
Water Bottle	-	3/5	-	3/5
Total	20/20	59/100	21/30	100/150

TABLE II: Accuracy of grasp type proprioception on the test object set. For the "distal" and "both" grasp types, objects are grasped off a table. For the "proximal" grasp type, objects are handed to the gripper. We do not include trials with grasps that are not stable or have mixed contact types.

REFERENCES

[1] Josie Hughes, Utku Culha, Fabio Giardina, Fabian Guenther, Andre Rosendo, and Fumiya Iida. Soft manipulators and grippers: A review. *Frontiers in Robotics and AI*, 3:69, 2016.

[2] Matthew Mason. Toward robotic manipulation. *Annual Review of Control, Robotics, and Autonomous Systems*, 1(1), 2018.

[3] Zexiang Li and Shankar Sastry. Task-oriented optimal grasping by multifingered robot hands. *IEEE Journal on Robotics and Automation*, 4(1):32–44, 1988.

[4] Mariangela Manti, Vito Cacucciolo, and Matteo Cianchetti. Stiffening in soft robotics: A review of the state of the art. *IEEE Robotics & Automation Magazine*, 23(3):93–106, 2016.

[5] Xianpai Zeng and Hai-Jun Su. A high performance pneumatically actuated soft gripper based on layer jamming. *Journal of Mechanisms and Robotics*, 15(1), 2023.

[6] Hang Wei, Yu Shan, Yanzhi Zhao, Lizhe Qi, and Xilu Zhao. A soft robot with variable stiffness multidirectional grasping based on a folded plate mechanism and particle jamming. *IEEE Transactions on Robotics*, 38(6):3821–3831, 2022.

[7] Yang Yang, Yazhan Zhang, Zicheng Kan, Jielin Zeng, and Michael Yu Wang. Hybrid jamming for bioinspired soft robotic fingers. *Soft robotics*, 7(3):292–308, 2020.

[8] Revanth Konda, David Bombara, Steven Swanbeck, and Jun Zhang. Anthropomorphic twisted string-actuated soft robotic gripper with tendon-based stiffening. *IEEE Transactions on Robotics*, 39(2):1178–1195, 2022.

[9] Loai AT Al Abeach, Samia Nefti-Meziani, and Steve Davis. Design of a variable stiffness soft dexterous gripper. *Soft robotics*, 4(3):274–284, 2017.

[10] Yang Yang, Yingtian Li, and Yonghua Chen. Principles and methods for stiffness modulation in soft robot design and development. *Bio-Design and Manufacturing*, 1(1):14–25, 2018.

[11] Lael Odhner et al. A compliant, underactuated hand for robust manipulation. *IJRR*, 33(5):736–752, 2014.

[12] James Bern, Fatemeh Zargarbashi, Annan Zhang, Josie Hughes, and Daniela Rus. Simulation and fabrication of soft robots with embedded skeletons. In *ICRA*. IEEE, 2022.

[13] Saeed Hashemi, Darrin Bentivegna, and William Durfee. Bone-inspired bending soft robot. 8(4):387–396, 2021.

[14] Ryan Truby et al. Soft somatosensitive actuators via embedded 3d printing. *Advanced Materials*, 30(15), 2018.

[15] R Adam Bilodeau, Edward White, and Rebecca Kramer. Monolithic fabrication of sensors and actuators in a soft robotic gripper. In *IROS*. IEEE, 2015.

[16] Javier Tapia, Espen Knoop, Mojmir Mutnỳ, Miguel A Otaduy, and Moritz Bächer. MakeSense: Automated sensor design for proprioceptive soft robots. *Soft robotics*, 7(3):332–345, 2020.

[17] Tao Jin et al. Triboelectric nanogenerator sensors for soft robotics aiming at digital twin applications. *Nature Communications*, 11(1):5381, 2020.

[18] Aaron Dollar and Robert Howe. The SDM hand: A highly adaptive compliant grasper for unstructured environments. In *ISER*. Springer, 2009.

[19] Nicolas Rojas, Raymond Ma, and Aaron Dollar. The GR2 gripper: An underactuated hand for open-loop in-hand planar manipulation. *IEEE Transactions on Robotics*, 32(3):763–770, 2016.

[20] Mariangela Manti, Taimoor Colette, Giovanni Passetti, Nicolò D'Elia, Cecilia Laschi, and Matteo Cianchetti. A bioinspired soft robotic gripper for adaptable and effective grasping. *Soft Robotics*, 2(3):107–116, 2015.

[21] Byungchul Kim, Hyunki In, Dae-Young Lee, and Kyu-Jin Cho. Development and assessment of a hand assist device: GRIPIT. *Journal of neuroengineering and rehabilitation*, 14: 1–14, 2017.

[22] Ankit Bhatia, Aaron Johnson, and Matthew Mason. Direct drive hands: Force-motion transparency in gripper design. In *RSS*, 2019.

[23] Behzad Babaei, Ali Davarian, Kenneth M Pryse, Elliot L Elson, and Guy M Genin. Efficient and optimized identification of generalized maxwell viscoelastic relaxation spectra. *Journal of the mechanical behavior of biomedical materials*, 55:32–41, 2016.

[24] Bruno Belzile and Lionel Birglen. A compliant self-adaptive gripper with proprioceptive haptic feedback. *Autonomous Robots*, 36:79–91, 2014.

[25] Bruno Belzile and Lionel Birglen. Stiffness analysis of underactuated fingers and its application to proprioceptive tactile sensing. *IEEE/ASME Transactions on Mechatronics*, 21(6):2672–2681, 2016.

[26] Bruno Belzile and Lionel Birglen. Stiffness analysis of double tendon underactuated fingers. In *ICRA*. IEEE, 2014.

[27] Useok Jeong and Kyu-Jin Cho. Feedforward friction compensation of bowden-cable transmission via loop routing. In *IROS*. IEEE, 2015.

[28] Russ Tedrake and the Drake Development Team. Drake: Model-based design and verification for robotics, 2019. URL `https://drake.mit.edu`.

[29] Josie Hughes, Shuguang Li, and Daniela Rus. Sensorization of a continuum body gripper for high force and delicate object grasping. In *ICRA*. IEEE, 2020.

[30] Ryoji Maruyama, Tetsuyou Watanabe, and Masahiro Uchida. Delicate grasping by robotic gripper with incompressible fluid-based deformable fingertips. In *IROS*. IEEE, 2013.